Remote Sensing of Environment 113 (2009) 2689–2700

Contents lists available at ScienceDirect

Remote Sensing of Environment

journal homepage: www.elsevier.com/locate/rse

Validation of a SeaWiFS dust-correction methodology in the Mediterranean Sea: Identification of an algorithm-switching criterion

V.F. Banzon [a,*], H.R. Gordon [b], C.P. Kuchinke [b], D. Antoine [c], K.J. Voss [b], R.H. Evans [a]

[a] RSMAS/MPO, University of Miami, 4600 Rickenbacker Cswy, Miami, FL 33133, USA
[b] Dept. of Physics, University of Miami, Coral Gables, FL 33124, USA
[c] Laboratoire d'Océangraphie de Villefranche, 06230 Villefranche su mer, France

ARTICLE INFO

Article history:
Received 24 April 2009
Received in revised form 3 August 2009
Accepted 7 August 2009

Keywords:
SeaWiFS
Dust
Atmospheric correction
Spectral matching algorithm
Mediterranean sea
Dust correction
BOUSSOLE
AOPEX cruise
Algorithm
Satellite bias
Water leaving radiance
Aerosol models

ABSTRACT

A spectral matching algorithm (SMA) that allows atmospheric correction in the presence of dust aerosols is applied to SeaWiFS imagery in the northwest Mediterranean Sea. The goal is to find criteria that could be used to identify SMA target pixels and to gain insights into the method's accuracy relative to the standard SeaWiFS processing scheme (STD). This work also represents the first validation of SMA using *in situ* data. The validation dataset includes water-leaving radiances collected from both a fixed buoy site and from a ship during the Advanced Optical Properties Experiment (AOPEX) cruise in August 2004. Supplementary information was provided by the ship LIDAR and coastal AERONET stations in Villefranche (France) and Blida (Algeria) that recorded aerosol conditions near the buoy and proximal to the dust sources, respectively. Backward aerosol transport trajectories were also available for the AERONET sites, allowing identification of potential dust sources, especially for aerosol layers observed by the LIDAR. Over the study period, four aerosol events affected the buoy vicinity, but SMA retrievals proved superior to standard processing results only when dust was dominant, rather than when dust was simply present. The conditions appropriate for an SMA application could be defined using AERONET parameters. They are a combination of high aerosol optical depth τ_a and low Ångström exponent α (or $\tau_a/\alpha > 0.2$). Similar results are obtained using the equivalent SeaWiFS parameters produced by the STD method although the threshold value is different. Since it is preferable to apply the criterion on a per-pixel basis prior to atmospheric correction to select SMA or STD processing, an analogous test using aerosol model-independent quantities derived from SeaWiFS data is proposed. Thus, SMA and STD processing can be applied to a single image, where appropriate.

1. Introduction

Current standard atmospheric correction methodology (STD; Gordon and Wang, 1994; details in Section 1.3.2) for retrieving water-leaving radiances (L_w) from ocean color satellite measurements is not appropriate when absorbing aerosols, such as Saharan dust, are present (e.g., Carder et al., 1991; Gordon et al., 1997; Fukushima et al., 2000; Moulin et al., 2001b; Schollaert et al., 2003). Consequently, a dust-compensating algorithm would have a far-reaching impact by significantly increasing data coverage over dust-impacted waters, hence providing a more complete dataset for climate change and other analyses. In order to successfully implement a dust-correction algorithm for ocean color on an operational basis, the principal requirements are: 1) a set of region-specific models that represent the range of local dust aerosol properties, 2) a computational procedure to estimate the aerosol properties (e.g., through model selection or interpolation between models), and 3) a criterion for selecting the target pixels so that other methodologies can be applied to the non-dusty parts of the image. Globally speaking, STD performs well in the presence of the most common scattering aerosol types, so the dust-specific approach needs to be applied only when the retrieval error represents an improvement over that of STD.

With regard to the first two requirements, this work represents a validation effort for a pre-existing methodology and associated dust models. Over the years, various approaches to dust correction of ocean color data have been proposed (e.g., Gordon et al., 1997; Fukushima et al., 2000; Carder et al., 1991), but none have been adopted into mainstream processing. In this study, we use the spectral matching algorithm (SMA; Gordon et al., 1997; described in Section 1.3.3) that was developed for the Sea-Viewing Wide Field of View Sensor (SeaWiFS) and an associated set of Saharan dust models (Moulin et al., 2001a). Prior to this work, SMA has not been validated with *in situ* data, but recently available datasets now make this feasible (as discussed in Section 1.2). However, the principal focus of this work is to understand the conditions associated with a smaller SMA retrieval error relative to STD, and thus, develop a robust criterion for deciding when to apply SMA.

* Corresponding author.
E-mail address: vbanzon@rsmas.miami.edu (V.F. Banzon).

0034-4257/$ – see front matter © 2009 Elsevier Inc. All rights reserved.
doi:10.1016/j.rse.2009.08.007

The SeaWiFS dataset represents the longest well-characterized chlorophyll *a* (CHL) time series from 1997 to present. It constitutes a significant part of the satellite record that has been used to identify long-term trends (e.g., Antoine et al., 2005; Gregg et al., 2005). SeaWiFS has six visible bands: (412, 443, 490, 510, 555, 670 nm) and two near-infrared (NIR) bands: (765, 865 nm), from which aerosol and in-water parameters are computed. An error in the atmospheric correction process (that permits computation of L_w; Section 1.3) will inevitably propagate to CHL that is computed from L_w band-ratios (Gordon, 1997). On a global basis, the SeaWiFS CHL error over optically deep water is ~26% but increases to ~33% with the inclusion of coastal data (Bailey and Werdell, 2006). This is a result of the increase in the L_w error from ca.11–16% (for the 412 to 555 nm bands) over open water to 16%–24 % (with essentially no change for the 555 nm band and the greatest impact on the 412 nm band) with coastal data included. The pervasive occurrence of absorbing aerosols such as dust in coastal areas has been proposed as a possible explanation for this wavelength-dependent change in L_w error (Bailey and Werdell, 2006).

As explained by Gordon et al. (1997), for the case of more strongly-absorbing aerosols, the STD approach cannot be improved by simply adding more models to the available set because the NIR bands, used in the STD method to select aerosol models, do not distinguish between weakly- and strongly-absorbing aerosols. In addition, the influence of strongly-absorbing aerosols depends on their vertical distribution, which is usually unknown. For dust aerosols in particular, absorption in the visible part of the spectrum decreases as wavelength increases (e.g., Dubovik et al., 2002; Cattrall et al., 2003), and thus can have a significant influence on bands important for the computation of CHL. While various masking criteria are typically applied to avoid processing pixels where STD retrievals are not possible or reliable, the screening process is not foolproof. Anomalous data halos are often observed at the edges of dust plumes (e.g., Cropp et al., 2005; Volpe et al., 2009). Thus, an effective SMA implementation should target pixels not only in the region currently masked, but also in the parts of the image that are not masked but have strongly biased values (due to dust presence) when processed with STD methods.

To identify target pixels, it would be advantageous to use quantities derived from SeaWiFS such that the test is always available for each pixel during processing. The most obvious candidates are absorbing aerosol indices that use SeaWIFS bands proposed by Nobileau and Antoine (2005) and Hsu et al. (2000). However, both of these published indices do not discriminate between dust and pollution-type aerosols. Another possibility is to use SeaWIFS-derived aerosol parameters. Since these are products of the aerosol computation, but need to be used before the atmospheric correction process, this creates a circular problem. Our approach is to first examine aerosol quantities measured by an independent instrument to identify the best test criterion. On this basis, we can then identify the more rudimentary SeaWiFS parameters that are available before the aerosol computation.

1.1. Objectives

The general objective of this paper is to apply SMA to the western Mediterranean Sea and evaluate its performance (relative to STD) using a unique *in situ* dataset of aerosol and in-water measurements. The ulterior goal is to use the retrieval errors to identify a test criterion for identifying the SMA target pixels. Towards this goal, the sub-objectives are: 1) to characterize atmospheric conditions in terms of various parameters, e.g., vertical structure, potential aerosol sources, atmospheric optical depth, with special attention to dust events; 2) to compare the errors in STD and SMA retrievals of in-water upwelling radiance (L_w) using *in situ* measurements as reference; 3) to relate SMA errors to the atmospheric parameters (defined in Section 1.3) such as Ångström exponent, single scattering albedo and aerosol optical depth; and 4) to identify the best predictor of improved retrievals using SMA (relative to STD and sea truth). Finally, this work seeks to gain insights into future improvements that can make an operational dust-correction algorithm a reality.

1.2. The study area

The Mediterranean Sea is ideal for this study due to the frequency of dust occurrences and the availability of a wide range of *in situ* data. Dust events in this region are cyclone-driven and thus, smaller in spatial scale than those in the Atlantic where large-scale prevailing winds determine the dust transport patterns (Engelstaeder et al., 2006 and references therein). Thus, within a short time span, it is possible to obtain data under a range of atmospheric conditions, from clear to dust-dominated. Under the "BOUée pour l'acquiSition d'une Série Optique à Long termE" (or BOUSSOLE) project, bio-optical measurements from a fixed buoy (43° 22′ N, 7° 54′ E; Fig. 1; also referred to as site B) have been collected since 2001 (Antoine et al., 2006). Moreover, in August 2004, complementary ship-based observations were made during the Advanced Optical Properties Experiment (AOPEX cruise). For the same period, data from the Aerosol Robotic Network (AERONET; Holben et al., 1998) is available for coastal stations in Villefranche (France), about 30 miles north of site B, and in Blida (Algeria) proximal to the dust source region (Fig. 1). Thus, the August 2004 period presented a unique opportunity to have a relatively complete picture of in-water and aerosol conditions at the study area.

The choice of the Mediterranean as a study site was also advantageous because it permitted the use of Saharan dust models that had been developed for use with SMA (Moulin et al., 2001a). The Saharan desert is the main dust source in the Mediterranean. However, absorbing aerosols other than dust can also be present. It is not known at what point the dust models used in the SMA become inappropriate, but multi-site observations do show that the optical properties of a dust layer are altered along its trajectory due to aging and interaction with other types of aerosols (Balis et al., 2006). Like dust, industrial aerosols tend to introduce a negative bias in L_w, resulting in an overestimate of CHL (Chomko and Gordon, 2001). However, the two aerosol types differ in their spectral behavior: pollution-type aerosols tend to be strongly absorbing at all visible wavelengths, unlike dust for which absorption increases with decreasing wavelength (Shettle and Fenn, 1979; Cattrall et al., 2003). To correct for pollution-type aerosols, a different methodology (e.g., spectral optimization or SOA; Chomko and Gordon, 2001; details in Section 1.3.4) is more appropriate. One of the examples presented in this paper examines a situation where SOA produced better retrievals than SMA or STD. It should also be noted that in the Mediterranean Sea, the global SeaWIFS chlorophyll algorithm does not

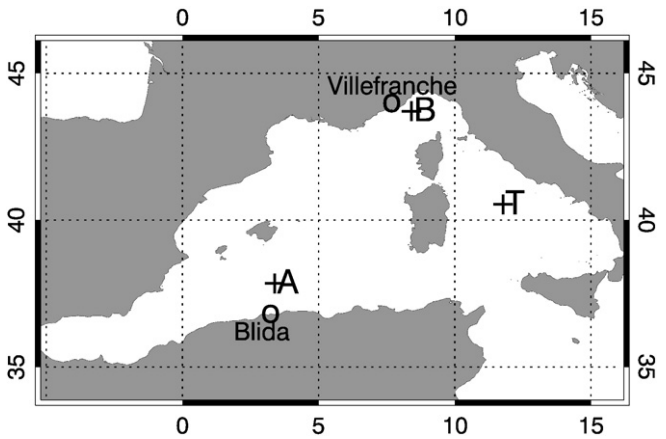

Fig. 1. Map of the Western Mediterranean Sea shows offshore sites B, T and A (crosses) and coastal AERONET stations (circles). The AOPEX cruise was focused on both sites B and T, while the fixed buoy measurements were almost continuous at site B. No *in situ* measurements were made at Site A, but it was arbitrarily selected to examine the satellite in-water and aerosol retrievals close to dust source areas.

perform well due to the particular optical properties of the waters (e.g., Volpe et al., 2007 and references therein). Our study focuses only on L_w to evaluate SMA, although the ship-based pigment measurements are useful in describing the typical conditions at the sampled stations and in identifying anomalous satellite and buoy L_w results.

1.3. Atmospheric correction

1.3.1. General considerations

After removing the effects of sun glint and surface roughness, the total radiance measured by the satellite L_T can be expressed as:

$$L_T = L_r + L_a + t\,L_w, \tag{1}$$

where L_w is the water-leaving radiance, L_r and L_a are contributions due to Rayleigh and aerosol scattering (the latter including the Rayleigh–aerosol interaction as well), respectively, and t is the diffuse transmittance through the atmosphere. While accurate L_r can be computed by incorporating ancillary data, e.g., the surface atmospheric pressure, L_a is difficult to estimate because it varies with aerosol type, and in the case of absorbing aerosols, with aerosol vertical structure. Note that when L_w can be ignored, L_a can be approximated by $L_A = L_T - L_r$, a quantity sometimes referred to as the Rayleigh-removed total radiance. In remote sensing it is usually more convenient to use reflectance rather than radiance. The reflectance ρ corresponding to a radiance L is defined by $\rho = \pi L/(F_0 \cos\theta_0)$, where F_0 is the instantaneous solar irradiance at the top of the atmosphere, and θ_0 is the angle between a vector directed from the sea surface to the sun, and the local zenith, e.g., $\rho_a = \pi L_a/(F_0 \cos\theta_0)$, *etc.*

To understand the parameters that are important in atmospheric correction, it is useful to examine the single scattering approximation to L_a or equivalently, ρ_a. At a particular wavelength λ_i, the aerosol reflectance in the single scattering approximation is given by (after Gordon, 1997)

$$\rho_a(\lambda_i) = \frac{\omega_o(\lambda_i)\tau_a(\lambda_i)p_a(\theta_v,\phi_v;\theta_0,\phi_0;\lambda_i)}{4\cos\theta_v\cos\theta_0} \tag{2}$$

where

$$p_a(\theta_v,\phi_v;\theta_0,\phi_0;\lambda_i) = P_a(\Theta_-,\lambda_i) + [r(\theta_v) + r(\theta_0)]P_a(\Theta_+,\lambda_i), \tag{3}$$

$P_a(\Theta,\lambda_i)$ is the aerosol phase function for scattering through an angle Θ, $r(\theta)$ is the Fresnel reflectance of the sea surface for light incident at an angle θ, and

$$\cos\Theta_\pm = \pm\cos\theta_v\cos\theta_0 - \sin\theta_v\sin\theta_0\cos(\phi_v - \phi_0) \tag{4}$$

with θ_0 and θ_v, respectively, the angle between a vector directed from the sea surface to the sun and the sensor, and ϕ_0 and ϕ_v, the corresponding azimuth angles of the two vectors. $\tau_a(\lambda_i)$ is the aerosol optical thickness at λ_i, and $\omega_o(\lambda_i)$ is the single scattering albedo (the ratio of aerosol scattering to aerosol extinction) at λ_i. The τ_a is a measure of the aerosol concentration, while the Ångström exponent α (*i.e.*, the slope of wavelength dependence of τ_a, expressed in exponential coordinates):

$$\alpha(\lambda_1,\lambda_2) = \log_e((\tau_a(\lambda_1))/\tau_a(\lambda_2))/\log_e(\lambda_2/\lambda_1) \tag{5}$$

is related to aerosol size: the larger the particles, the smaller the value of α (Ångström, 1929). The single scattering albedo is a measure of the aerosol's absorption ability: unity for a non-absorbing aerosol and zero for a non-scattering aerosol. Typical values are 1.0 for a maritime aerosol (Shettle and Fenn, 1979), 0.8–0.9 for dust in the blue (Cattrall et al., 2003), and 0.5 for pure carbonaceous aerosol (Shettle and Fenn, 1979). Thus, the effectiveness of an atmospheric correction scheme depends on how well $\omega_o(\lambda_i)$, $\tau_a(\lambda_i)$, and $P_a(\Theta,\lambda_i)$, are represented. These are the aerosol parameters we focus on in our results.

1.3.2. The standard algorithm (STD)

The STD atmospheric correction procedure for SeaWiFS compensates for the effects of the most common global aerosols that range from weakly to non-absorbing types (details in Gordon and Wang, 1994; Wang, 2000). These aerosols are characterized by ω_o and $P_a(\Theta)$ that vary very weakly with wavelength, as reflected in the suite of 12 candidate aerosol models currently in use (Wang, 2000). The STD models are named by aerosol type (O = oceanic, M = marine, C = continental, T = tropospheric) and relative humidity level (e.g., M50 for a marine aerosol type at 50% relative humidity). For most of the world ocean, CHL concentrations are low and L_w can be neglected in the NIR. Thus, using Eq. (1) for the two NIR bands, L_a can be computed. Note that for high chlorophyll regions, the NIR L_w is not negligible but may be estimated by a bio-optical model (e.g., Siegel et al., 2000). A best-fit test is applied to the NIR L_a results to select two aerosol models, and their relative contributions (weights) are computed based on the fit error. Using Eq. (2) and the weights, an average $\tau_a(865)$ is computed. To complete the atmospheric correction procedure, the L_a obtained from the NIR bands are propagated to the visible wavelengths using the derived aerosol models and τ_a, and the corresponding L_w values are obtained using Eq. (1). For SeaWIFS, α is typically computed using Eq. (5) for $\lambda_1 = 510$ nm referenced to $\lambda_2 = 865$ nm or simply $\alpha(510,865)$.

1.3.3. The spectral matching algorithm (SMA)

Unlike the STD algorithm that first computes L_a to obtain L_w, SMA utilizes all the ocean color bands to simultaneously estimate aerosol and in-water biophysical properties (details in Gordon et al., 1997). As in the STD procedure, a set of candidate aerosol models are employed, each characterized by a respective ω_o and $P_a(\Theta)$. In addition, a Case 1 waters bio-optical model relates L_w to both CHL and a particle scattering parameter b^0 (Gordon et al., 1988). Thus, for each aerosol model, it is possible to compute $L_a + tL_w$ for each spectral band, as a function of CHL, b^0, and the aerosol optical thickness in the NIR, $\tau_a(865)$. The optical thickness appropriate to a given aerosol model can be determined assuming that $L_w(865) = 0$. Then, exercising the model for a discrete set of CHL and b^0 values and each aerosol model, a comparison is made between the measured $L_a + tL_w = L_T - L_r$, and that estimated from the model. The final parameter set (including an aerosol model) is that which minimizes the square of the difference between the measured and the computed values of $L_a + tL_w$ summed over all of the spectral bands. Note that CHL value in the solution set is not used further but the L_w can be used as input into the CHL algorithm of choice.

Gordon et al. (1997) demonstrated the effectiveness of SMA using synthetic data representing various absorbing aerosol types. To specifically use SMA for dust-compensation in SeaWIFS imagery, Moulin et al. (2001a) developed a set of 18 models representing a combination of two spectrally-varying refractive indices (called BDS and BDW, depending on whether published or optimized Saharan dust values are used, respectively), three size distributions (1 = small to 3 = large), and three dust column heights (2, 4, 6 km). The dust models used in the SMA context allowed Moulin et al. (2001b) to successfully produce a spatially and temporally consistent sequence of pigment maps with reduced spatial gaps for the northwestern African coast, a region frequently traversed by Saharan dust plumes. A similar application to the Arabian Sea produced a unique time series documenting the phytoplankton bloom during the southwest monsoon, when the satellite view of the Omani coast is normally obscured by dust for several months (Banzon et al., 2004). More recently, the SMA code has been embedded into the SeaWiFS Data Analysis System (SeaDAS), widely used for processing SeaWIFS imagery which has well-maintained calibration and temporal degradation information. Prior to this, a straightforward evaluation of SMA products relative to STD results could not be made. A significant limitation of the SMA is that it does not perform well if the suite of aerosol models contains

both strongly absorbing and non-absorbing aerosols, *i.e.*, for a successful application some knowledge of the aerosol type is required. Thus, a simple test within the SeaWiFS processing scheme is needed to determine when the dust models (used in the SMA context in this study) might be appropriate, and ideally, the decision needs to be made before the atmospheric correction process.

1.3.4. The spectral optimization algorithm (SOA)

A second absorbing aerosol algorithm — the spectral optimization algorithm (SOA) — was proposed by Chomko and Gordon (2001) to handle pollution-type aerosols, *i.e.*, carbonaceous aerosols. This algorithm is similar to the SMA; however, no attempt is made to model the aerosol size distribution in a detailed manner. Instead, a simple Junge-type power law distribution, specified by a single parameter υ (developed by Chomko and Gordon, 1998) is used to represent aerosol absorption. In addition, the refractive index of the particles is taken to be independent of wavelength. Through interpolation a continuum of aerosol models are obtained. The original SOA used the Gordon et al. (1988) bio-optical model (as in the SMA). Subsequent SOA versions are presented in Chomko et al. (2003) and Kuchinke et al. (2009). The latter version, that is used in this study, also employs the Garver and Siegel model (Garver and Siegel, 1997; Maritorena et al., 2002). This bio-optical model uses CHL, the absorption coefficient of dissolved organics and detrital particles at 443 nm, and the backscattering coefficient of particles at 443 nm to specify L_w. As in the SMA, the SOA attempts to find the best fit between the computed and measured $L_a + tL_w$. However, rather than using the trial and error method of the SMA, the best fit is determined using standard optimization techniques.

Thus, SMA is designed for dust because the refractive index depends on wavelength and SOA is designed for pollution-type or carbonaceous aerosols because the refractive index is relatively independent of wavelength.

2. Data and methods

2.1. In situ measurements

Daily values of normalized-water-leaving radiance L_{wN} were obtained from the BOUSSOLE fixed buoy (site B; Fig. 1). Incident light (E_s) and water-leaving radiance (L_w) were measured using Satlantic OCR200 series instruments with seven channels (Antoine et al., 2008). In this study, data from Aug. 6 to 25, 2004 (herein referred to as the August deployment) is used, with measurements for the 412, 443, 490, 510, 560, 665 and 683 nm bands. For this study, the 412, 443 and 490 nm data were the most desirable since dust retrieval errors are expected to be greater in the blue region. Using 10-minute averaged data, L_w were normalized using E_s. The normalized-water-leaving radiance L_{wN} is then derived as described in Gordon and Clark (1981). L_{wN} is approximately the radiance that would exit the water in the absence of the atmosphere and with the sun at the zenith. For the satellite matchups, a daily L_{wN} value was obtained by averaging all data from 1000 to 1400 GMT, which represented the SeaWiFS overpass time window.

Ship-based measurements of L_{wN} were collected during the AOPEX cruise, conducted from July 31–Aug. 17, 2004 aboard the vessel *Le Suroit*. The E_s and L_w were measured using a Satlantic SeaWiFS Multichannel Surface Reference (SMSR) and a free-fall Satlantic SeaWiFS Profiling Multichannel Radiometer (SPMR), respectively. As with the buoy data, L_{wN} was computed. Other data and observations are described in greater detail Antoine et al. (2006) or detailed in the ship log. On-board atmospheric instruments included a Micro-pulse LIDAR (Spinhirne et al., 1995) that collected data continuously and permitted detection of high-backscattering aerosol layers. The LIDAR data product reported here is the normalized relative backscatter (NRB; Welton, 1998).

The ship-based bio-optical measurements were focused on two locations: 1) site B, and 2) site T (40° 12′ N, 11° 17′ E; Fig. 1). The ship occupied site T on Aug. 5–10, and was at site B on July 31–Aug. 3 and Aug. 12–17. Site T is located in the Tyrrhenian Sea which is known to be more oligotrophic compared to the Ligurian Sea where the buoy is located (e.g., Volpe et al., 2007; Bosc et al., 2004). During the AOPEX cruise, the average CHL concentration at site T was 0.07 mg m^{-3} and 0.11 mg m^{-3} at site B (or about 1.5 times greater than site T), based on HPLC analyses. Ship-based L_{wN} values were also higher at site T than at site B, particularly for the first three wavelengths (Table 1) consistent with the lower CHL concentrations at site T.

In this work, the *in situ* L_{wN} datasets are the reference used to evaluate the results of the two satellite processing approaches. Thus, it is important to establish that the both datasets were consistent with each other. Our focus was to validate the daily buoy values (*i.e.*, the 1000–1400 GMT average) that represented a longer time series and thus potentially more satellite matchups. In contrast, the ship data were very sparse (between one to three measurements per day) from which a daily average was computed regardless of the time. Buoy and ship measurements overlapped at site B for only 3 days during which the means of the two datasets were generally similar (Table 2). The average L_{wN} values from the ship tended to be slightly lower than those from the buoy, but the difference was less than 5% for the shorter wavelengths (412, 443 and 490 nm bands). The greatest discrepancy was observed at 510 nm, for which the ship value was about 16% lower than the buoy value.

While comparisons over the AOPEX period indicated that the ship and buoy datasets agree at site B for the three shortest bands for which dust absorption is greatest, the buoy 412 nm L_{wN} exhibited a slight but significant decreasing trend over the August deployment period (with a linear regression slope of −0.017, μW cm^{-2} sr^{-1} nm^{-1} d^{-1}, and r^2 of 0.60). A possible explanation for the trend is bio-fouling or detector degradation, which is particularly troublesome for the short wavelengths. It may also indicate an increase in colored dissolved organic matter (CDOM), which has particularly strong absorption at 412 nm. Although no CDOM measurements were made during AOPEX, one of the authors (D. Antoine) has data from other periods that suggest it can be important at site B. Due to concerns regarding the 412 nm channel, most of the SMA error evaluation in this work are shown in terms of the 443 nm data.

AERONET data from stations in Villefranche (43° 41′ 02″ N, 7° 19′ 44″ E) and Blida, Algeria (36° 30′ 28″ N, 02° 52′ 51″ E) were used to

Table 1
Mean daily $L_{wN}(\lambda)$ at sites T and B (units = μW cm^{-2} sr^{-1} nm^{-1}) at two study sites during the AOPEX cruise.

λ=	412	443	490	510	555	670
Site						
T $n=4$	1.68 (0.12)	1.62 (0.10)	1.15 (0.08)	0.62 (0.05)	0.24 (0.02)	0.04 (0.00)
B $n=4$	1.19 (0.14)	1.16 (0.11)	1.00 (0.07)	0.67 (0.03)	0.29 (0.01)	0.019 (0.001)

Standard deviations are shown in parentheses. Locations are shown in Fig. 1.

Table 2
Mean daily $L_{wN}(\lambda)$ at Site B for days that measurements were available from both the ship and buoy (units = μW cm^{-2} sr^{-1} nm^{-1}).

λ=	412	443	490	510	560	665
Platform						
Buoy	1.19	1.17	1.01	0.72	0.31	0.020
$n=3$	(0.06)	(0.04)	(0.04)	(0.04)	(0.03)	(0.004)
Ship	1.18	1.11	0.98	0.62	0.26	0.026
$n=3$	(0.07)	(0.03)	(0.03)	(0.01)	(0.01)	(0.001)

Standard deviations are shown in parentheses.

assess atmospheric conditions in the vicinity of site B and near the dust source region, respectively. AERONET aerosol properties are derived using a flexible inversion algorithm by fitting the entire measured radiance field at four wavelengths (440, 670, 870 and 1020 nm) to a radiative transfer model (Dubovik and King, 2000). We used AERONET Level 2.0 products that are calibrated, cloud-screened, and quality checked (Smironov et al., 2000). Among the numerous AERONET parameters, the daily aerosol optical depth at 870 nm [τ_a(870)] and the Ångström exponent estimated over the 500 to 870 nm range [α(500, 870)] were selected to coincide with analogous STD SeaWiFS products [τ_a(865) and α(510, 865)]. The AERONET back trajectory analyses at 1200 GMT, for four pressure levels (950, 850, 700 and 500 hPa, which approximately correspond to 0.5, 1.5, 3.0 and 5.0 km altitude, respectively), were also used to infer aerosol sources.

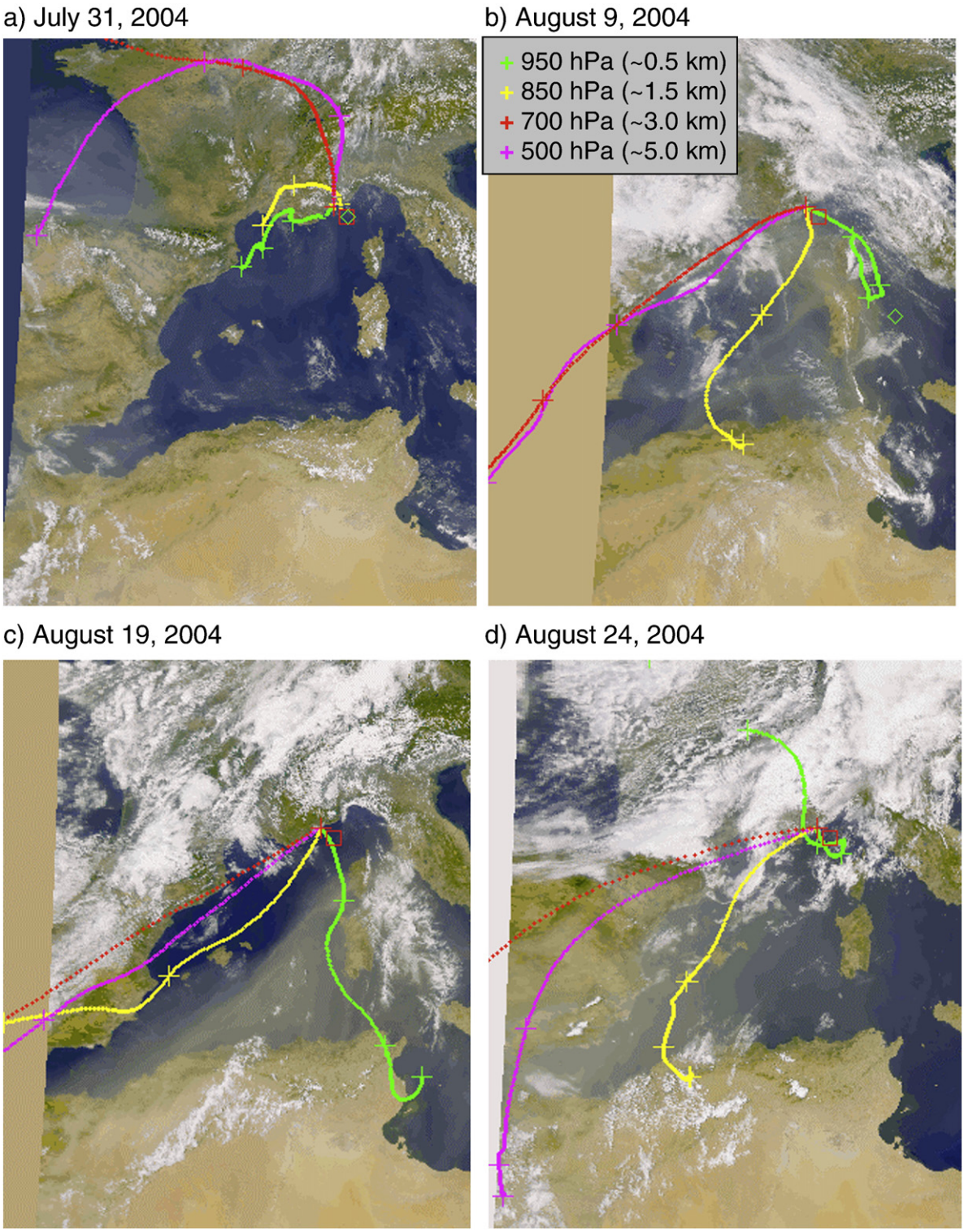

Fig. 2. SeaWIFS quasi-true color images representing four aerosol events that affected Villefranche and vicinity: a) Jul. 31, 2004, b) Aug. 9, 2004, c) Aug. 19, 2004 and d) Aug. 24, 2004. Backward trajectories originate from Villefranche: large crosses = 1200 GMT of each day. See legend for pressure levels and equivalent altitude. Other symbols: red square = fixed buoy (site B); green diamond = AOPEX cruise ship location on specific day.

AERONET inversion products such as the single scattering albedo and phase function were also examined to evaluate the performance of the three SeaWIFS processing algorithms. AERONET data and documentation regarding products, retrieval algorithms, cloud screening, quality control, *etc.* can be found at http://aeronet.gsfc.nasa.gov.

2.2. Satellite data processing

All algorithms (STD, SMA and SOA) were processed within SeaDAS 5.1 to ensure that they used the same radiometric calibration. Level 1 SeaWiFS MLAC passes from July 31 to Aug. 27, 2004 covering the Western Mediterranean were processed using STD methods, while SMA was applied only to selected passes corresponding to dust event periods affecting site B. Candidate dust events were identified by prior visual inspection of true color images. In the latter part of the work, SOA was also applied to selected passes to investigate if unsatisfactory SMA results during some dust events might be due to the influence of industrial aerosols, in which case SOA should produce better results.

For processing to Level 2 data, only the land mask was activated, while other masking criteria were applied *a posteriori*. Since the default suite of flags (atmospheric correction failure, sun glint, total radiance above knee value, high satellite zenith angle, stray light, clouds/ice) tended to exclude most of the SMA target pixels, alternate masking criteria were explored. Dust is highly reflective and tends to activate some flags in particular, i.e., cloud/ice, total radiance above knee value, stray light. The latter two are intimately tied to the instrument characteristics and were not modified since results tended to be noisier when these flags were not applied. The SeaWiFS cloud/ice test is based on albedo and excludes pixels with $\rho_a(865) > 0.027$. By relaxing the threshold value to 0.075 in this study, moderately dusty pixels could be processed while pixels containing white clouds and very thick dust were disqualified. However, an additional homogeneity test was introduced to minimize spurious results along large $\rho_a(865)$ gradients (typically cloud edges). The minimum and maximum $\rho_a(865)$ within a 3×3 box centered on the pixel of interest were determined. If this difference exceeded 0.04, the pixel was excluded. This produces very similar results to a test based on the standard deviation (higher values mean less homogeneity) used by Moulin et al. (2001b) but requires less computation.

To evaluate L_{wN}, the satellite values co-located with the *in situ* data were extracted to produce the matchup dataset, following Bailey and Werdell (2006) with some modifications. *In situ* observations within ±3 h of a pass were used rather than the recommended two-hour time window to allow inclusion of more ship data, which were sparse. If more than one ship measurement was available, the one closest to the satellite overpass time was used. Pixel values within a 5×5 box centered on the *in situ* location were extracted. Averages and related statistics were computed after excluding invalid pixels identified using the appropriate flags. Matchups were discarded if less than 9 pixels were valid.

To compare with the AERONET data at sites B, T and A, the SeaWiFS aerosol parameters within the 5×5 pixel box centered on the desired location were extracted, similar to the in-water matchups. The methodology for computing an average matchup value differed depending on whether STD, SMA or SOA were used. While τ_a is a routine product for all methods, ω_o and $P_a(\Theta)$ had to be approximated. With STD and SMA processing, each candidate aerosol model has an associated ω_o and $P_a(\Theta)$. For each pixel, STD writes out the two bracketing aerosol models selected but not their relative weights. Thus, average ω_o and $P_a(\Theta)$ are computed separately for all the upper limit models (the so-called aermodel_max) and all the lower limit models (aermodel_min), and the two curves are shown in the results (e.g., Fig. 7a–b). In the case of SMA, only one model is selected per pixel and thus, the associated ω_o and $P_a(\Theta)$ are simply averaged. SOA estimates a size distribution parameter υ and ω_o for the 865 nm band. The mean observed ω_o is used to select the closest model ω_o from the possible combinations (six imaginary by two real refractive indices) associated with the closest υ. For the selected combination of parameters, there is also a corresponding $P_a(\Theta)$.

3. Results

3.1. Atmospheric events

Over the study period, four distinct atmospheric events were observed in the Ligurian Sea area, where both Site B and Villefranche are located. Representative quasi-true color SeaWiFS images show that the first event had a whitish haze (Fig. 2a). For the other three events, dust plumes had a characteristic brown color (Fig. 2b–d). For each event, AERONET $\tau_a(870)$ at Villefranche exhibited a peak (Fig. 3a). The

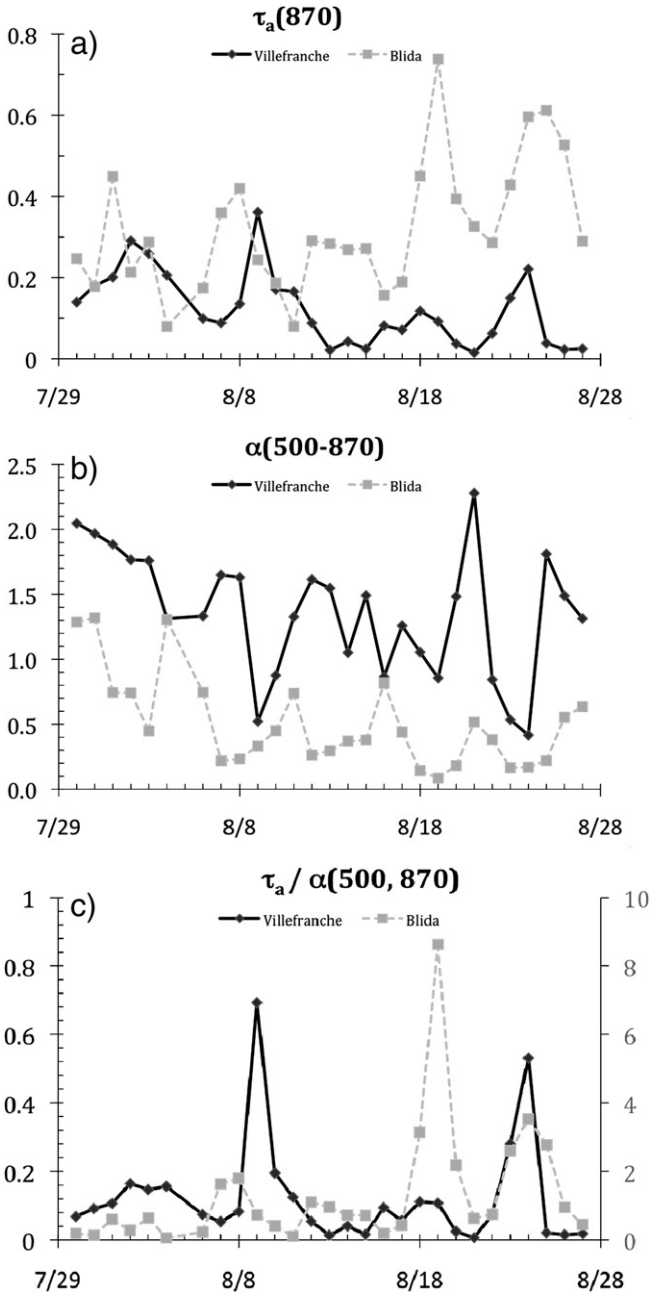

Fig. 3. AERONET daily mean values for a) $\tau_a(870)$, b) $\alpha(500, 870)$ from coastal stations at Villefranche and Blida, and c) $\tau_a(870)/\alpha(500, 870)$ with vertical scale on left (right) for Villefranche (Blida).

second one (Aug. 9) had the highest maxima (Fig. 3a). A comparison with $\tau_a(870)$ patterns at the AERONET station in Blida provide an indication of how efficiently African dust events propagated to the northwest Mediterranean. Fig. 3b shows five distinct $\tau_a(870)$ peaks at Blida all characterized by low $\alpha(550,870)$ that is indicative of dust dominance. Only the second Blida maximum (Aug. 8) corresponds to a peak of almost the same intensity at Villefranche, after a one-day lag. For the rest of the study period, the peaks in $\tau_a(870)$ at Villefranche rarely exceeded 0.3, and were generally lower than those at Blida. While the most intense events at Blida occurred on Aug. 19 and 27, these events corresponded to weak events at Villefranche. One Blida event (Aug. 12–14) did not even produce an equivalent peak in Villefranche, probably because the plume trajectory was blocked by a meteorological front. Aerosol events at the two AERONET locations were not always related. Examination of the SeaWiFS quasi-true color time series (not shown) suggests the first $\tau_a(870)$ peak at Villefranche is not connected to a Blida event.

The aerosol size composition, as indicated by $\alpha(550,870)$, was almost always different at the two AERONET stations (Fig. 3b). The $\alpha(550,870)$ values were lower at Blida (mostly <0.5), suggesting a predominance of coarse-sized aerosols, as compared to Villefranche, where values (>1.0) suggested a persistent fine particle dominance. At Blida, $\alpha(550,870)$ values exceeding 1.0 occurred only during the first event. In contrast, coarse particles dominate at Villefranche [$\alpha(550,870) \sim 0.5$] only during the single day peaks of Aug. 9 and Aug. 24. Thus, background aerosol levels at Villefranche are lower than Blida but have more significant fine particle contribution.

Finally, Fig. 3c provides the ratio of $\tau_a(870)$ to $\alpha(550,870)$ for the two stations. Clearly, this ratio is useful in discriminating dust from other aerosols, with high values indicating dust. This will be used as the basis of a test proposed for choosing STD or SMA in dust-prone regions.

3.2. Ship aerosol observations and AERONET back trajectory analysis

Ship LIDAR observations, used together with back trajectories from Villefranche, show the heights of aerosol layers during the AOPEX cruise, and potential aerosol source areas. Fig. 4a shows 3 days of LIDAR profiles at site B during the first event. Multiple aerosol layers (from near-surface and up to 4.5 km altitude) were present on July 30 and 31. The LIDAR results are consistent with the ship log that reported an absence of clouds but poor eye-level visibility for the 2 days, with conditions changing on Aug. 1 to significant cumulus cloud coverage. High backscatter was observed at ~1 km height on the first 2 days. On July 30, a broad aerosol layer was also present at 1.5 to 4.0 km altitude. By mid-day Aug. 1, this strong backscatter was concentrated at 1.5 km altitude while a weaker but distinct signal also occurred at the 3–4 km level (Fig. 4a). The July 31 back trajectory analysis at 1200 GMT (Fig. 2a) suggests aerosols below 2 km came from nearby sources, while the air mass at ~3.0 km approached from the north, having originated over the Atlantic where a dust storm had passed in previous days. This path over Europe can bring in industrial aerosols, and could explain the dominance of fine particles indicated by the AERONET data.

For the second event (Fig. 4b), the three-day LIDAR observations at site T indicate the passing of a dust plume, also consistent with the ship log. A strong backscattering layer (ca. 3 km height) appears at noon on Aug. 8. It appears to descend over the next 2 days, with aerosol backscatter also increasing down to the sea surface, suggesting settling. The height of the aerosol maximum varies over each day but we focus on the vertical structure at 1200 GMT on Aug. 8 and 9 in order to relate with the back trajectories from Villefranche in Fig. 2b. Back trajectories from Villefranche for Aug. 9 at 1200 GMT indicate that aerosols at 1.5 km altitude probably have originated from Algeria 2 days earlier, while those above 3 km came from the Atlantic, coast off Africa, possibly Morocco or the Western Sahara. The surface layer has a local origin although the path goes out to the Tyrrhenian Sea, then returns. Note that the SeaWiFS image shows a general haziness with zones of thick brown dust, rather than a well-defined plume, suggesting dust transport may be occurring in more than one layer (Fig. 2b).

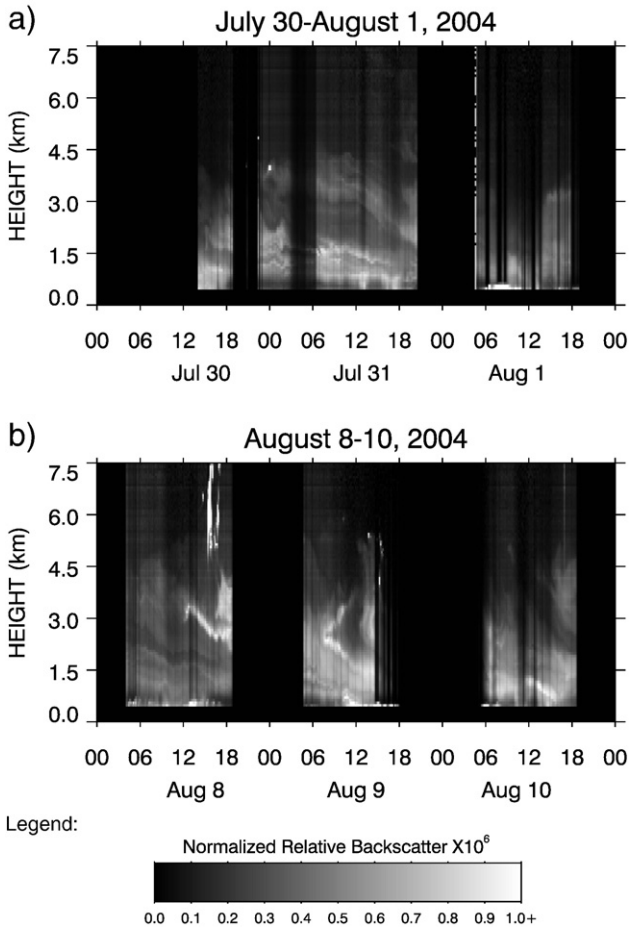

Fig. 4. Three-day atmospheric LIDAR profiles centered on: a) the July 31 event ats site B; b) the Aug. 9 event at site T. Time for each day is in GMT. Normalized relative backscatter (NRB) is reported in relative units × 106.

No LIDAR data are available to identify the aerosol layer heights for the last two events but back trajectories are still informative. For the third event (Aug. 19; Fig. 4c), trajectories above 1.5 km are parallel to the well-defined western dust plume edge, suggesting that the dust transport is probably occurring at these heights and that the main dust plume is kept south of Villefranche by a front. The upper layer trajectories pass over the Iberian peninsula, where marine, and to a lesser extent, continental and pollution-type aerosols are typical (Pace et al., 2006). The surface layer trajectory, that traces back to Tunisia, appears to be causing a light smearing of the dust plume northward over the Ligurian Sea (Fig. 2c), but AERONET data presented earlier shows the dust does not reach Villefranche (Fig. 3a–b). For the fourth event (Aug. 24; Fig. 2d), the dust cloud is diffuse, and backward trajectories suggest two potential dust sources. The air mass at 1.5 km altitude would have originated from Algeria, while that at 3 km comes from the border between southwest Algeria and Morocco. The surface layer traces back to Northern Europe, a source of fine particles. Thus, back trajectories suggest a fine particle contribution for all four atmospheric events in Villefranche, which would explain the higher $\alpha(500, 870)$ reported for Villefranche compared to Blida in Fig. 3b.

3.3. In situ and satellite water-leaving radiance comparisons

In situ L_{wN} matchups with the SeaWiFS data were obtained mostly at site B. Out of the 25 days of buoy measurements, 13 valid matchups were found. For the ship data, there were five valid matchups, only one of which was at site T. The plot of the difference between the satellite and *in situ* retrievals for 443 nm band over the study period shows that STD processing results were in good agreement with *in situ* data except on the dust-dominated days (Fig. 5). The results are equivalent for the 412 and 490 bands (not shown). The difference between the STD and *in situ* L_{wN} (443) was generally small, on the order of 0.1 μW cm^{-2}sr^{-1}nm^{-1} (Fig. 5). The biggest errors in STD processing occurred on Aug. 19, 9, and 23, in increasing order, at the height of the dust events. If the default L2 flagging criteria were used, the latter 2 days would have had no STD matchups, but the Aug. 19 value was not disqualified by the flags since the dust is very thin (Fig. 2c). Thus, use of the default flagging criteria in a dust-affected region like the Mediterranean appears to be able to effectively screen out bad data when dust is thick, but does not automatically guarantee reliable satellite retrievals when the dust is thinner. This would be consistent with the error halos at the boundary of dust plumes previously noted in STD CHL images (e.g., Cropp et al., 2005).

The SMA matchups shown are fewer than the STD results since only periods with high atmospheric turbidity were considered. The L_{wN}(443) differences show that SMA performed better than STD processing on Aug. 9, 19, and 23 (Fig. 5) which coincide with the aerosol events detected at the AERONET station in Villefranche, with $\alpha(550,870) < 0.9$ and $\tau_a(870) > 0.09$. It should be pointed out that that the Aug. 9 matchup is at site T. This is closer to the source region than Villefranche, such that the atmospheric conditions may actually be more dusty than reflected by the AERONET data. In contrast, SMA did not perform well during the first event when finer aerosols dominated and on days prior to or following the dust event peaks. These results strongly suggest that in climatologically dust-affected regions, SMA should be applied when dust particles are dominant rather than when dust is simply present.

The relation of the SMA error to the coincident aerosol parameters was examined to explore possible criteria for selecting pixels for SMA processing. Thus far, atmospheric parameters that give information about size appear to be related to the magnitude of the SMA error. A test based on ρ_a was examined since this quantity is computed without using any aerosol models. The $\rho_A(510)$ to $\rho_A(670)$ ratio, which is roughly analogous to the absorbing aerosol index of Nobileau and Antoine (2005), showed a trend but had too much variability making it difficult to define a critical value. In addition, no good relation was obtained for either the SeaWIFS $\tau_a(865)$ or the AERONET $\tau_a(870)$, that are both measures of aerosol concentration. As shown in Fig. 6a–b, the SMA retrieval error clearly increased with α (and thus decreasing aerosol size). This is not surprising since in the Mediterranean, the only important coarse-sized aerosol is dust. However, the relation is better defined when the AERONET estimate is used (Fig. 6b) rather than the equivalent SeaWIFS product (Fig. 6a). It is clear that the SMA retrievals improve with increasing $\tau_a(865)/\alpha(510,865)$ as measured by SeaWiFS (Fig. 6c) or the similar quantity as measured by AERONET (Fig. 6d). Importantly, Fig. 6e shows that replacing the SeaWiFS-estimated $\tau_a(865)$ by the SeaWiFS-measured $\rho_A(865)$, which is *aerosol model-independent*, serves as well as the parameters in Fig. 6c and d in predicting situations in which atmospheric correction will be improved using the SMA (along with the dust models). Similar results (not shown) were obtained at site A, that was characterized by a wider range of $\rho_a(865)/\alpha(510,865)$, but in lieu of *in situ* data, the monthly average $L_{wN}(443)$ was used to compute the satellite retrieval error.

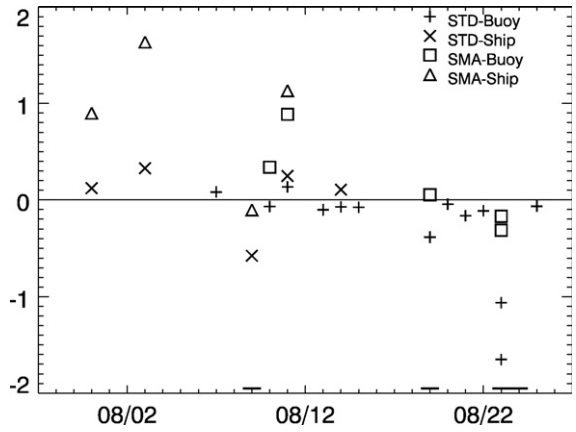

Fig. 5. Errors in STD and SMA L_{wN}(443) retrievals relative to coincident *in situ* measurements from ship (site B and T) and buoy (site B). SMA was applied only during atmospheric events and produced smaller error than STD ones during dust-dominated periods (indicated by thick lines in bottom, i.e., AERONET $\tau_a(870) > 0.1$ and $\alpha(500–870) < 0.90$ at Villefranche). Units in μW cm^{-2}sr^{-1}nm^{-1}.

3.4. Model selection and aerosol properties

Next, consider the single scattering albedo, ω_o as computed by the different atmospheric correction methods at different locations within a dust plume. In this comparison, AERONET retrievals can be used for reference, in the absence of more appropriate measurements, but it should be borne in mind that the on-ground AERONET instrument is upward-looking, while the satellite sensor looks downward, and therefore the two need not agree perfectly. The comparisons are limited because AERONET ω_o from the Villefranche station were available for very few days over the study period, and only on Aug. 9 among the dusty days. Moreover, on that day, there were no valid satellite matchups at site B, so only observations at sites T and A could be compared. Previously, it has been demonstrated that the critical quantity in atmospheric computation is ω_o, whereas large errors in P_a have little impact (Gordon, 1997; Chomko and Gordon, 1998). Thus, our main interest was to compare ω_o produced by the different methods at the two locations.

At each site, the STD ω_o values are essentially almost invariant with wavelength since this is the basic characteristic of the predominantly scattering models. But the SMA ω_o values vary greatly with wavelength. Site A (offshore of Blida) represents the case where coarse particles frequently dominate. Here, the SMA ω_o values were generally higher (0.87–0.97) than the AERONET result (0.80 to 0.90) but the wavelength-dependent curves were similar in shape (Fig. 7a). Thus, close to the dust source, SMA provided a better approximation of the aerosol properties than STD. Site T represents less dense atmospheric dust conditions than site A, and the closest AERONET data is from Villefranche. At site T, the SMA results changed significantly with wavelength in contrast with the less variable AERONET curve (Fig. 7b). The SMA result is particularly interesting in that the least absorbing model was selected for all 25 pixels. Thus despite the presence of a dust layer in site T (inferred from the ship LIDAR data and AERONET back trajectories from Villefranche), none of the dust models used in the SMA context could represent conditions at site T. The SOA method, which is more suitable for industrial aerosols (common air masses of European origin; Pace et al., 2006), was applied to test whether it would perform better. As shown in Fig 7b, the SOA ω_o was more similar in shape to the AERONET retrieval compared to the STD and SMA curves, although the values were offset.

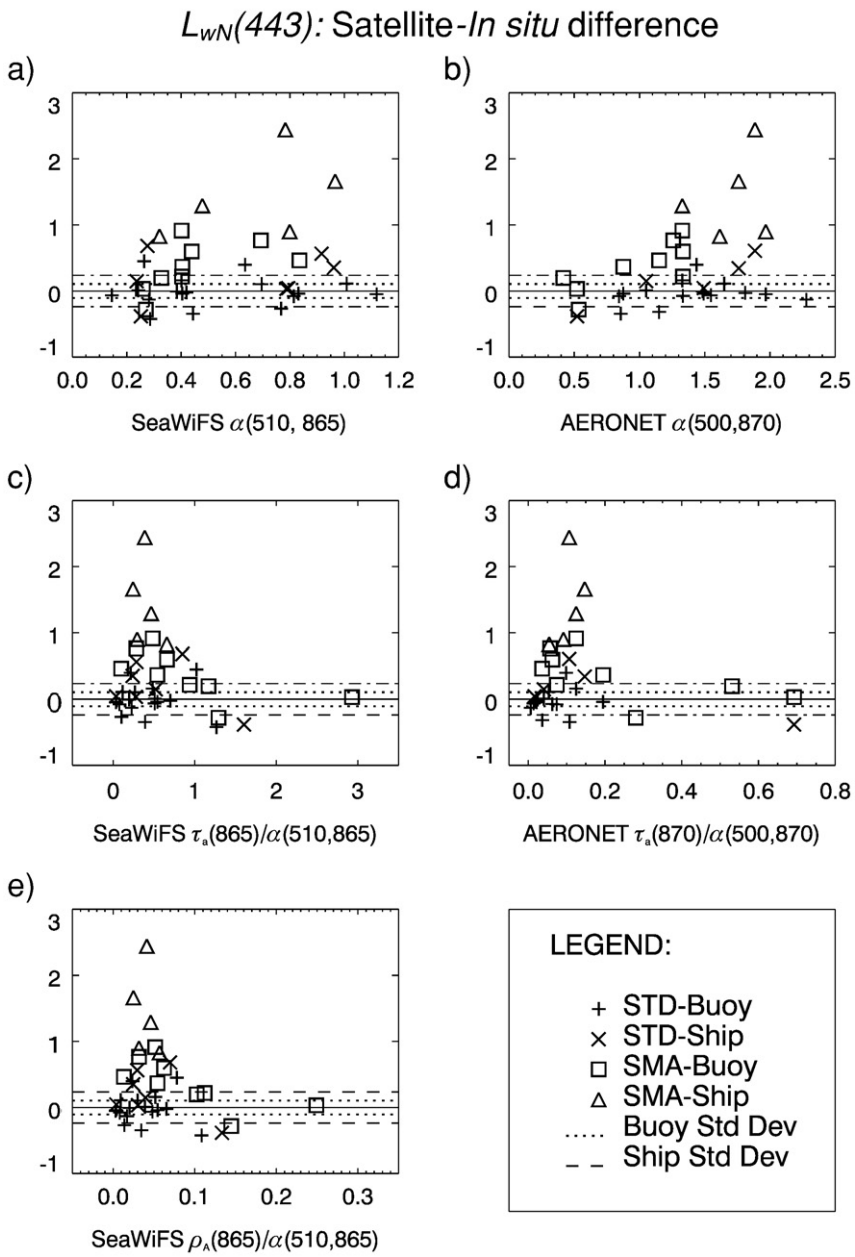

Fig. 6. $L_{wN}(443)$ STD and SMA retrieval errors (relative to *in situ* values) plotted against a) STD $\alpha(510, 865)$; b) AERONET $\alpha(500,870)$; c) STD $\tau_a(865)/\alpha(510,865)$; d) AERONET $\tau_a(870)/\alpha(500,870)$; e) STD $\rho_a(865)/\alpha(510,865)$. *Y*-axis in μW $cm^{-2} sr^{-1} nm^{-1}$. Symbols explained in legend.

4. Discussion

This work addresses the three requirements towards an operational implementation of a dust-correction algorithm for SeaWiFS. The more novel part of this effort was developing a criterion for selection of the most appropriate atmospheric correction methodology for each pixel. Previous work had been done on candidate Saharan dust models and methodology, so the efforts on these two were focused on validation using *in situ* data. Over a decade has passed since Gordon et al. (1997) first proposed SMA as a method for compensating for dust aerosols in ocean color satellite imagery. The general assumption was that if dust were present, a method such as SMA would produce reliable values. Thus, when this study was initiated, SMA was expected to provide better retrievals than the standard (STD) atmospheric correction procedure during dust events in the northwestern Mediterranean Sea, and that an associated challenge would be to determine where dust was present. During the four weeks examined in this study, dust was present during the four atmospheric events, as inferred from ship LIDAR backscatter, AERONET back trajectories, and/or visual inspection of SeaWiFS imagery. But contrary to expectations, the SMA retrieval error (relative to the *in situ* data) during these events was smaller than that of STD processing in only three matchups. In order to explain this, it was necessary to compare the aerosol properties at Villefranche (near the buoy) and Blida (close to the dust source). The comparison revealed that coarse particles (*i.e.*, dust) were generally dominant in Blida (Figs. 2 and 3c), while in Villefranche, dust was the predominant aerosol [as indicated by $\tau_a(870)/\alpha(500, 870) > 0.5$, Fig. 3c] only on the 1–2 day peak periods within dust events. Thus, although dust plumes were common in the northwest Mediterranean, the total column aerosol properties were rapidly modified such that the Saharan dust models were not always appropriate.

It is important to consider the candidate dust models in the context of the SMA procedure and the SeaWiFS instrument capabilities. Recall

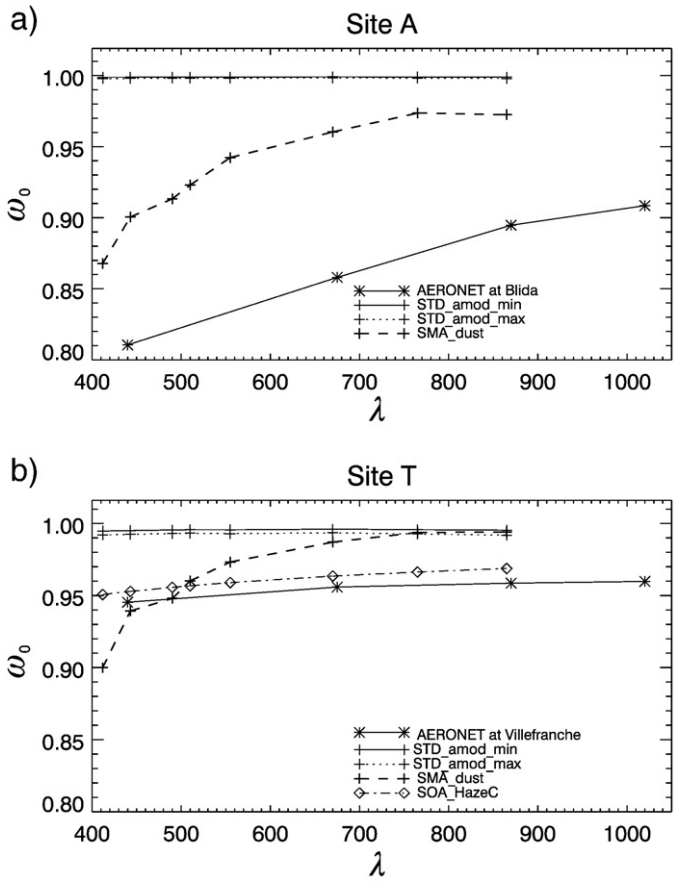

Fig. 7. Single scattering albedo ω_o on Aug 9, 2004 (SeaWiFS image at 1136 GMT) averaged over the 5×5 matchup box: a) at site A using STD and SMA processing and b) at site B using STD, SMA and SOA processing. The two STD curves represent the upper and lower brackets (amod_min and amod_max, respectively).

that the version of SMA used in this study selects only one model rather than performing an interpolation between two models (as in the STD method). An examination of the output model fields indicates that only a few of the candidate models are chosen for majority of the valid pixels. Invariably, at the outer part of the dust plume, models associated with the optimized refractive index (BDW) are more frequently chosen, while under thicker dust, the other group of models representing literature-based Saharan dust properties (BDS) is selected. The thick dust region is extremely highly reflecting, a condition that results in saturation of some or all of the SeaWiFS detectors (also associated with exceeding the "knee value" in the bilinear gain; Barnes et al., 1994). Since the data in this thick dust region are not utilizable, the number of BDS-type dust models could be reduced. One could consider that out of the 18 available dust models, any one selected less than 5% of the time is of limited use. Moulin et al. (2001a) examined the number of occurrences when a given dust model was the "best" choice (the one with the smallest residual relative to CZCS climatology) and found that only 10 models were the "best" choice over 5% of the time. Over 10% of the time, only two BDS models and three BDW models were selected. This suggests there is room for optimization of choices in the model suite. Moreover, for other regions of the world, a different suite of candidate models may be more appropriate and will need to be developed and validated with *in situ* data.

Another issue is that the difference in aerosol absorption among SMA dust models is much more significant than the differences across STD models (Fig. 7). Thus, although SMA produced more reasonable L_{wN} fields than the STD method within the dust-dominated area, there were noticeable spatial discontinuities coinciding with the change in the selected SMA model. An attempt to eliminate the discontinuities was made by using the weighted average of the closest 10 dust models to estimate aerosol parameters, but this merely smoothed the patterns. Aside from the pronounced ω_o difference across SMA dust models, the difference in shape and magnitude of ω_o between the STD and SMA models will also tend to produce noticeable discontinuities if the algorithms are applied to different parts of the same image. The SOA approach has greater flexibility in dealing with a continuum, and may be more versatile in dealing with mixed aerosol gradients. However, a different parameter continuum needs to be developed to make SOA suitable for dust applications.

It is important to recall that prior to this work, there was no quantitative test to identify the SMA target pixels. But the concept was to apply SMA on dust-affected pixels that are: 1) STD-processed but have biased retrievals, or 2) not processed because of flagging by the default masking criteria. With regard to the first type of target pixels, our validation exercise provided some insights on the STD masking tests and processing in a dust-impacted region. The default flagging criteria effectively screens out bad data when dust is thick, but not consistently when dust is less dense. In the latter case, the erroneously elevated CHL values may be misinterpreted as a dust-induced bloom (Volpe et al., 2009). Thus, for dust-impacted areas, the default masking criteria represent a necessary but insufficient condition for producing reliable CHL fields. For this reason, target pixel criterion is essential to the dust-correction algorithm implementation.

Once the actual atmospheric conditions were better understood, it was not surprising that the SMA success was limited in this study. Visual inspection of true color satellite images can indicate dust presence, but a more reliable SeaWiFS-based indicator of dust dominance — $\tau_a 865/\alpha(510, 865)$ — should be used to decide when to apply SMA. Many other studies have noted that dust events are characterized by high τ_a and low α (e.g., Pace et al., 2006; Smironov et al., 2002). This study extends this observation by proposing the use of τ_a/α as the basis for a SeaWiFS data processing test. In the initial evaluation, AERONET data was used to have aerosol parameters completely independent from SeaWiFS (Fig. 6b, d). The SMA error clearly was acceptable when the AERONET-derived $\tau_a(870)/\alpha(500, 870)$ exceeded ~0.2 (Fig. 6d). Unfortunately, the AERONET value is a point measurement, and it remains to be determined how to apply the value to the rest of the pixels in the image in order to decide which should be processed using SMA. However, Fig. 6e suggests that for SeaWiFS, $\rho_a(865)/\alpha(510, 865)$, that can be approximated in a straightforward manner without using any aerosol models, appears to be an excellent candidate for assessing the appropriateness of SMA in dust-prone regions. Our results suggest that the threshold: $\rho_a(865)/\alpha(510, 865) > 0.08$ to 0.10 would be a good indicator of when to switch to SMA. [Also note that a pseudo Ångström exponent can be estimated using $\rho_a(765)$ and $\rho_a(865)$ in Eq. (5), *i.e.*, pseudo $\alpha = \log_e(\rho_a(765)/\rho_a(865)/\log_e(865/765)]$.

5. Concluding remarks

In this study, the spectral matching algorithm (SMA) for SeaWiFS is tested in the Western Mediterranean Sea. Validation with *in situ* water-leaving radiances showed that SMA did not consistently perform better than the standard (STD) atmospheric correction algorithm when dust was present, but did when dust was the dominant aerosol, as indicated by AERONET data (high aerosol optical thickness and low Ångström exponent). This observation served as the basis for developing a test to select target pixels for SMA processing, using analogous but aerosol model-independent quantities from SeaWiFS. This allows the choice between SMA and STD processing to be made prior to the atmospheric correction step, and thus represents a significant step towards the blending of different types of processing in a single image. Obviously, Saharan dust models used in this work may not be suitable for other parts of the world and so there will be a need to develop region-specific aerosol models. Expectations of increased retrievals also have to be

moderated since the condition for SMA applicability, i.e., dust dominance, is less widespread than dust presence.

The insights obtained in this study would not have been possible without continuous observations in a dust-impacted area. Clearly, the multi-year BOUSSOLE dataset is invaluable in providing a comprehensive dataset for testing dust-compensating and other alternative atmospheric correction algorithms. The coupling with the nearby Villefranche AERONET station is a great asset, but the presence of the Blida AERONET station closer to the dust source was also essential in providing insights into how total column aerosol properties are modified over space and time. More coincident in-water and aerosol measurements are needed to verify the applicability of these results worldwide.

Finally, additional work will be required to minimize the spatial discontinuities resulting from switching between algorithms and among dust models, as well as the transition between the dust-dominated and mixed aerosol conditions. This may be achieved either by modifying the SMA candidate model set, or by adopting the optimization approach (SOA-like) along a continuum of dust-compatible aerosol parameters. For completeness, an analogous criterion for inclusion of SOA processing ultimately will be needed to address the blending of these multiple atmospheric correction methodologies.

Acknowledgements

The BOUSSOLE project is funded by the *Centre National de la Recherche Scientifique* (CNRS), the *Institut National des Sciences de l'Univers* (INSU), the French space agency "*Centre National d'Etudes Spatiales*" (CNES), the European Space Agency (ESA-ESTEC/ESRIN), and the *National Aeronautics and Space Administration* (NASA) of the United States through a Letter of Agreement with the *Université Pierre et Marie Curie* (UPMC, Paris). The AERONET Villefranche station, maintained by one of the co-authors (D. Antoine), is supported by LOA-PHOTONS (CNRS, France). NASA supported KV, HG, VB and CK through contracts NNX08AH93A and NNG04HZ21C, and RE through contract NNG04HZ23C. We would also like to thank Brent Holben at NASA for establishing and maintaining the Blida AERONET station. and Tom L. Kucsera (SSAI) at NASA/Goddard for providing the back trajectories, available together with other AERONET products at http://aeronet.gsfc.nasa.gov. NASA provides SeaWiFS data and SeaDAS software at http://oceancolor.gsfc.nasa.gov.

References

Ångström, A. (1929). On the atmospheric transmission of sun radiation and on dust in the air. *Geografiska Annaler*, *11*, 156−166.

Antoine, D., Chami, M., Claustre, H., D'Ortenzio, F., Morel, A., Bécu, G., et al. (2006). BOUSSOLE : a joint CNRS-INSU, ESA, CNES and NASA Ocean Color Calibration And Validation Activity. NASA Technical memorandum N° 2006-214147, NASA/GSFC, Greenbelt, MD, 61 pp.

Antoine, D., D'Ortenzio, F., Hooker, S. B., Bécu, G., Gentili, B., Tailliez, D., et al. (2008). Assessment of uncertainty in the ocean reflectance determined by three satellite ocean color sensors (MERIS, SeaWiFS, MODIS) at an offshore site in the Mediterranean Sea (BOUSSOLE project). *Journal of Geophysical Research*, *113*, C07013. doi:10.1029/2007JC004472.

Antoine, A., Morel, A., Gordon, H. R., Banzon, V. F., & Evans, R. H. (2005). Bridging ocean color observations of the 1980's and 2000's in search of long-term trends. *Journal of Geophysical Research*, *110*. doi:10.1029/2004JC002620.

Bailey, S. W., & Werdell, P. J. (2006). A multi-sensor approach for the on-orbit validation of ocean color satellite data products. *Remote Sensing of the Environment*, *102*, 12−23.

Balis, D., Amiridis, V., Kazadzis, S., Papayannis, A., Tsaknakis, G., Tzortzakis, S., et al. (2006). Optical characteristics of desert dust over the Mediterranean during summer: a case study. *Annales Geophysicae*, *24*, 807−821.

Banzon, V. F., Evans, R. H., Gordon, H. R., & Chomko, R. M. (2004). SeaWiFS observations of the Arabian Sea southwest monsoon bloom for the year 2000. *Deep Sea Res. II*, *51*, 189−208.

Barnes, R. A., Holmes, A. W., Barnes, W. L., Esaias, W. E., McClain, C. R., & Svitek, T. (1994). SeaWiFS Pre-launch Radiometric Calibration and Spectral Characterization. In S. B. Hooker, E. R. Firestone & J. G. Acker (Eds.), *NASA Tech. Memo. 104566, Vol. 23* (55 pp). NASA Greenbelt Space Flight Center, Greenbelt, MD.

Bosc, E., Bricaud, A., & Antoine, D. (2004). Seasonal and interannual variability in algal biomass and primary production in the Mediterranean Sea, as derived from 4 years of SeaWiFS observations. *Global Biogeochemical Cycles*, *18*, GB1005. doi:10.1029/2003GB002034.

Carder, K. L., Gregg, W. W., Costello, D. K., Haddad, K., & Prospero, J. M. (1991). Determination of Saharan dust radiance and chlorophyll from CZCS imagery. *Journal of Geophysical Research*, *96*(D3), 5369−5378.

Cattrall, C., Carder, K. L., & Gordon, H. R. (2003). Columnar aerosol single-scattering albedo and phase function retrieved from sky radiance over the oceans: Measurements of African dust. *Journal of Geophysical Research*, *108*(D9), 4287. doi:10.1029/2002JD002497.

Chomko, R. M., & Gordon, H. R. (1998). Atmospheric correction of ocean color imagery: Use of the Junge power-law aerosol size distribution with variable refractive index to handle aerosol absorption. *Applied Optics*, *37*, 5560−5572.

Chomko, R. M., & Gordon, H. R. (2001). Atmospheric correction of ocean color imagery: Test of the spectral optimization algorithm with the Sea-viewing Wide Field-of-View Sensor. *Applied Optics*, *40*, 2973−2984.

Chomko, R. M., Gordon, H. R., Maritorena, S., & Siegel, D. A. (2003). Simultaneous retrieval of oceanic and atmospheric parameters for ocean color imagery by spectral optimization: A validation. *Remote Sensing of Environment*, *84*, 208−220.

Cropp, R. A., Gabric, A. J., McTainsh, G. H., & Braddock, R. D. (2005). Coupling between ocean biota and atmsopheric aerosols: Dust, dimethylsulphide, or artifact? *Global Biogeochemical Cycles*, *19*, GB4002. doi:10.1029/2004GB002436.

Dubovik, O., Holben, B. N., Eck, T. F., Smirnov, A., Kaufman, Y. J., King, M. D., et al. (2002). Variability of absorption and optical properties of key aerosol types observed in worldwide locations. *Journal of Atmospheric Science*, *59*, 590−608.

Dubovik, O., & King, M. D. (2000). A flexible inversion algorithm for retrieval of aerosol optical properties from sun and sky radiance measurements. *Journal of Geophysical Research*, *105*, 20673−20696.

Engelstaedter, S., Tegen, I., & Washington, R. (2006). North African dust emissions and transport. *Earth Science Reviews*, *79*, 73−100.

Fukushima, H., Toratani, M., Yamamiya, S., & Mitomi, Y. (2000). Atmospheric correction algorithms for ADEOS/OCTS ocean color data: Performance comparison base on ship and buoy measurements. *Advances in Space Research*, *25*, 1015−1024.

Garver, S., & Siegel, D. (1997). Inherent optical property inversion of ocean color spectra and its biogeochemical interpretation: 1 time series from the Sargasso Sea. *Journal of Geophysical Research*, *102C*, 18607−18625.

Gordon, H. R. (1997). Atmospheric correction of ocean color imagery in the Earth Observing System era. *Journal of Geophysical Research*, *102*(D14), 17081−17106.

Gordon, H. R., & Clark, D. K. (1981). Clear water radiances for atmospheric correction of coastal zone color scanner imagery. *Applied Optics*, *20*(24), 4175−4179.

Gordon, H. R., & Wang, M. (1994). Retrieval of water-leaving radiance and aerosol optical thickness over the oceans with SeaWiFS: A preliminary algorithm. *Applied Optics*, *33*, 443−452.

Gordon, H. R., Brown, O. B., Evans, R. H., Brown, J. W., Smith, R. C., Baker, K. S., et al. (1988). A semi-analytic radiance model of ocean color. *Journal of Geophysical Research, D*, *93*, 10909−10924.

Gordon, H. R., Du, T., & Zhang, T. (1997). Remote sensing of ocean color and aerosol properties: Resolving the issue of aerosol absorption. *Applied Optics*, *36*(33), 8670−8684.

Gregg, W. W., Casey, N. W., & McClain, C. R. (2005). Recent trends in global ocean chlorophyll. *Geophysical Research Letters*, *32*, L03606. doi:10.1029/2004GL021808.

Holben, B. N., Eck, T. F., Slutsker, I., Tanre, D., Buis, J. P., Setzer, A., et al. (1998). AERONET — A federated instrument network and data archive for aerosol characterization. *Remote Sensing of Environment*, *66*, 1−16.

Hsu, N. C., Robinson, W. D., Bailey, S. W., & Werdell, P. J. (2000). The description of the SeaWiFS absorbing aerosol index. In: S. B. Hooker & E. R. Firestone (Eds.), *SeaWiFS Postlaunch Technical Report Series, NASA Tech. Memo. 2000-206892, Vol. 10* (pp. 3–5). NASA Greenbelt Space Flight Center, Greenbelt, MD.

Kuchinke, C. P., Gordon, H. R., & Franz, B. A. (2009). Spectral optimization for constituent retrieval in Case 2 waters 1: Implementation and performance. *Remote Sensing of Environment*, *113*, 571−587. doi:10.1016/j.rse.2008.11.001.

Maritorena, S., Siegel, D. A., & Peterson, A. R. (2002). Optimization of semi-analytical ocean color model for global scale applications. *Applied Optics*, *41*, 2705−2714.

Moulin, C., Gordon, H. R., Banzon, V. F., & Evans, R. H. (2001). Assessment of Saharan dust absorption in the visible from SeaWiFs imagery. *Journal of Geophysical Research*, *106*(D16), 18239−18249.

Moulin, C., Gordon, H. R., Chomko, R. M., Banzon, V. F., & Evans, R. H. (2001). Atmospheric correction of ocean color imagery through thick layers of Saharan dust. *Geophysical Research Letters*, *28*, 5−8.

Nobileau, D., & Antoine, D. (2005). Detection of blue-absorbing aerosols using near infrared and visible (ocean color) remote sensing observations. *Remote Sensing of Environment*, *95*(3), 368−387.

Pace, G., di Sarra, A., Meloni, D., Piacentino, S., & Chamard, D. (2006). Aerosol optical properties at Lampedusa (Central Mediterranean). 1. Influence of transport and identification of different aerosol types. *Atmospheric Chemistry and Physics*, *6*, 697−713.

Schollaert, S. E., Yoder, J. A., O'Reilly, J. E., & Westphal, D. L. (2003). Influence of dust and sulfate aerosols on ocean color spectra and chlorophyll *a* concentrations derived from SeaWiFS off the U.S. east coast. *Journal of Geophysical Research*, *108*(C6), 3191. doi:10.1029/2000JC000555.

Shettle, E.P., & Fenn, R.W. (1979). Models for the aerosols of the lower atmosphere and the effects of humidity variations on their optical properties. AFGL-TR-79-0214, *Environmental Research Paper No. 675*, NTIS ADA 085951 (94 pp.). Air Force Geophysics Laboratory, Hanscomb AFB, MA 01731.

Siegel, D. A., Wang, M., Maritorena, S., & Robinson (2000). Atmospheric correction of satellite ocean color imagery: The black pixel assumption. *Applied Optics*, *39*, 3582−3591.

Smironov, A., Holben, B. N., Dubovik, O., O'Neill, N. T., Eck, T. F., Westphal, D. L., et al. (2002). Atmospheric optical properties in the Persian Gulf. *Journal of Atmospheric Sciences*, *59*, 620−634.

Smironov, A., Holben, B. N., Eck, T. F., Dubovik, O., & Slutsker, I. (2000). Cloud screening and quality control for the AERONET database. *Remote Sensing of Environment*, *73*, 337−349.

Spinhirne, J. D., Rall, J., & Scott, V. S. (1995). Compact eye-safe lidar systems. *Rev. Laser Eng.*, *23*, 26−32.

Volpe, G., Santoleri, R., Vellucci, V., Ribera d'Alcala, M., Marullo, S., & D'Ortenzio, F. (2007). The colour of the Mediterranean Sea: Global versus regional bio-optical algorithms evaluation and implication for satellite chlorophyll estimates. *Remote Sensing of Environment*, *107*, 625−638.

Volpe, G., Banzon, V. F., Evans, R. H., Santoleri, R., Mariano, J., & Sciarra, R. (2009). Satellite observations of the impact of dust in a low nutrient low chlorophyll region: Fertilization or artifact? *Global Biogeochemical Cycles*, *23*. doi:10.1029/2008GB003216.

Wang, M. (2000). The SeaWiFS atmospheric correction algorithm updates. In S. B. Hooker & E. R. Firestone (Eds.), SeaWiFS Postlaunch Technical Report Series, NASA Tech. Memo. 2000-206892, Vol. 9. (pp. 57–63). NASA Greenbelt Space Flight Center, Greenbelt, MD.

Welton, E.J. (1998). *Measurements of aerosol optical properties over the ocean using sunphotometry and lidar*. Ph.D. Dissertation. University of Miami, Coral Gables, 1-150.